

Optical Chiral Microrobot for Out-of-plane Drilling Motion

Alaa M. Ali^{1*}, Edison Gerena^{2,3*}, Julio Andrés Iglesias Martínez^{1*}, Gwenn Ulliac^{1*}, Brahim Lemkalli^{1*}, Abdenbi Mohand-Ousaid^{1*}, Sinan Haliyo^{2*}, Aude Bolopion^{1*}, Muamer Kadic^{1*}

¹Université de Franche-Comté, CNRS, Institut FEMTO-ST (UMR 6174), Besançon, 25000, France

²Sorbonne Université, CNRS, Institut des Systèmes Intelligents et de Robotique (UMR 7222 ISIR), Paris, France

³MovaLife Microrobotics, Paris, France

* alaa.ali@femto-st.fr

* edison.gerena@nova.life

* julioandres.iglesiasmartinez@gmail.com

* gwenn.ulliac@femto-st.fr

* brahim.lemkalli@femto-st.fr

* abdenbi.mohand@femto-st.fr

* sinan.haliyo@sorbonne-universite.fr

* aude.bolopion@femto-st.fr

* muamer.kadic@univ-fcomte.fr

Keywords: *Optical trapping, microrobots, optical forces*

Optical Microrobots (Optobots) have demonstrated a keen interest in various fields including microfluidics, microrobotics, and medicine. Conversely, optomechanics serves as a crucial domain for theoretical exploration into concepts such as chirality, duality, and parity concerning optical forces. In this paper, we elucidate a method to amalgamate chirality through broken axial parity into optobots, thereby augmenting their versatility. Specifically, we illustrate how this integration allows for out-of-plane rotation which helps in their utilization as optical drills under unidirectional excitation achieved through repetitive stimulation of three focal regions: two traps and one chiral rotational site. We fabricate the microrobots employing two-photon lithography, and note a highly satisfactory correspondence between finite element calculations and experimental observations.

1 Introduction

Light possesses the capability to exert force on objects by its energy and momentum. This phenomenon was initially recognized as far back as 1619 by Kepler, who observed the deflection of comet tails under the influence of sunlight [1]. Subsequently, the advent of lasers, which concentrate the power of light into a small area, facilitated significant progress in leveraging optical forces for the manipulation of microscopic objects [2, 3, 4]. Consequently, the inaugural optical tweezer was pioneered by Arthur Ashkin in 1970 [5, 6, 7]. Optical tweezers led to great discoveries and applications in different fields such as chemistry [8, 9, 10], nanotechnology [11, 12, 13, 14], Quantum Science [15], plasmonics [16], thermodynamics [17] and microrobotics [18, 19]. However, optical tweezers are most commonly used in biology and biophysics; they are used to trap and manipulate a single microorganism such as virus [20, 21] and bacterium [20, 22]; this can help in studying the interactions of these organisms with human cells.

The force exerted on an object per unit area, termed radiation pressure, is directly proportional to the rate of change of linear momentum. Traditionally, for objects of passive materials, this pressure moves the object in the direction of light flow. Recent advancements have demonstrated alterations in force direction, achieved through nontrivial tractor beams or asymmetrical and active materials [2]. This includes phenomena like optical pulling and lateral forces [4]. Additionally, torque can be induced through the angular momentum of light. Optical tweezers offer comprehensive control over microparticles. In essence, manipulation—be it trapping, rotation, or directional movement—can be effectively accomplished using Gaussian-like beams. The actuation of microrobots using optical tweezers has unlocked a realm of possibilities in the field of microrobotics. This technique has the advantage of applying the optical trap in specific points and control each one independently. Thus, control with high precision can be achieved and multiple degrees of freedom can be generated for the actuated microrobot. Although the biological cells

can be directly trapped by the optical tweezer, it is more favorable to control it using microrobots actuated by optical tweezers to avoid any harm to the cells that may be caused by the laser power, and this also helps in different applications such as cell puncture [23], cell rotation [24] and bio-mechanics studies [25].

Out-of-plane rotation of optical microrobots (optobots) is demanded especially for medical applications, as it is needed for cell drilling and handling in specific orientations for some microsurgeries and studies such as single-cell analysis, sperm injection, nuclear transplantation, and multi-dimensional imaging. Furthermore, it is also important for the control of the microfluidic chips to form pumps and micro-mixers. To achieve out-of-plane rotation, a holographic optical tweezer should be used. It relies on several focused light beams, each controllable individually. This allows for out-of-plane rotation by independently adjusting the depth of the focal point for various laser traps. Nevertheless, the holographic setup is complex, bulky, and costly [19]. Therefore, other simpler planar optical tweezer system based on time sharing techniques may be more favorable to be used. Time-sharing techniques depend on deflecting the laser beam between several trap positions with high frequency; this is achieved by using actuated mirrors, acousto-optic deflectors, or electro-optic deflectors. This allows the trapping of multiple objects or multiple parts of the microrobot at the same time and due to the high frequency of the trap position rotation, trapped particles do not have time to be lost from the trap. However, these techniques are very often limited to the planar motion of the traps [26].

Different designs of optobots were introduced in the literature to give out-of-plane rotation using planar optical tweezers. There are different approaches used to give out-of-plane rotation. The first approach depends on sequential trapping of a curved structure and by changing the distance between two traps, the orientation of the structure changes, and because it is curved this will induce out-of-plane rotation [19]. Another approach is using a structure with multi-components connected by joints. By trapping the base to fix it and moving another trap on the mobile head; this leads to its rotation due to the joint [27]; but, some optimisations are needed to avoid adhesion between the joint component. The third approach depends on the scattering force to push a paddle-wheel-like structure [28]; however, the rotation was nonuniform. Generally, the previously proposed designs are limited to either rotations without achieving a full cycle or low rotational velocity.

In this work, we depend on a different approach, which is based on chiral structures. Chirality refers to the asymmetrical geometric arrangement of components within a structure or system, resulting in a non-superimposable mirror image configuration such as springs which can either wind in a clockwise (right-handed) or counterclockwise (left-handed) direction when viewed along the axis of the spring. Chiral geometries in fluid mechanics can induce rotational motion or torque transmission when subjected to translational velocity, particularly in microscale systems dominated by viscous forces enabling applications such as microfluidic mixing, propulsion, and turbulence control [29]. Chiral structures were introduced before to induce rotations as a result of optical forces by controlling the polarization of the incident light beam; however, the rotations were in-plane [30, 31, 32, 33].

In this paper, we propose a microrobot that has two heads to trap from (optical handles) and a chiral tail (helix) so that when the laser is directed to it, out-of-plane rotation can be achieved by breaking the axial parity and by applying a constant off-axis force on the chiral part; resulting in a continuous rotation of the optobot. The principal is explained first, then the computational investigations and the experimental realisation.

2 Design of the Optobot

To design a functional optical drill, we must consider that the process uses an optical tweezer and is observed under a microscope; therefore, all components must be on the same plane. For instance, if a cell needs to be drilled, both the driller and the cell must be on the same plane to be observable under a single focal plane of the microscope. Consequently, the rotation of the driller must occur out-of-plane to drill something beside it. Additionally, the drilling process must be on-demand; thus, controlling the driller's translational motion and position must be separate from controlling its rotation. It is also preferable to be able to rotate the driller while it is either fixed or moving forward to effectively penetrate the object to

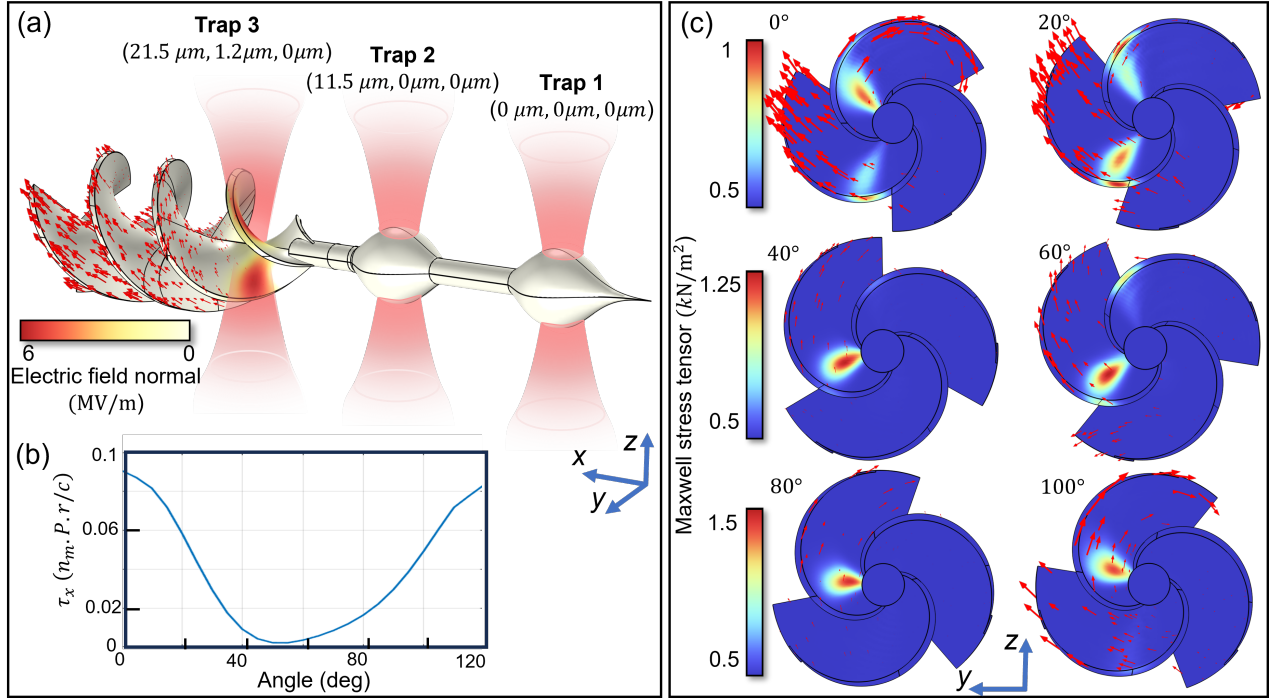


Figure 1: Principle of the Optical Drill. (a) Design of the Optobot showing the laser beams positions with their coordinates (Traps 1 to 3) onto it with propagation along the z -direction. Here, Trap 1 and 2 are used to hold the Optobot while the off-axis Trap 3 is used to create pressure on the optobot's helix and generate its rotation. We depict on the helix the norm of the electric field created by the Gaussian illumination via the false colorscale on its surface. (b) The rotation of the Optobot is only possible under a constant sign of the torque along the x -direction and we depict the normalized τ_x versus different angles occupied during a full revolution of the optobot, from 0 to 120 degrees (equivalent to the full rotation due to the C3 rotational symmetry of the structure). Where n_m is the refractive index of the medium (water), P is the laser power, r is the radius of the helix part interacting with the laser beam and c is the light velocity. This calculation is done while assuming the two other traps generate a stable stiffness and do not allow the Optobot to move and give the only possible motion a revolution along the x -axis. A positive value of τ_x is observed. In (c) we show the magnitude of the Maxwell stress tensor for different angles during the rotation, The color map is shown for each two angles, while the red arrows show the displacement field direction. The calculations were done assuming input laser power of 630 mW.

be drilled.

Our proposed microrobot has an arrow-like design (depicted in Figure 1(a)). Its head serves as an optical handle where the laser beam is directed to trap it, with two optical handles on the same axis (Trap 1 and Trap 2) to keep the microrobot in place. The tail is a helix with a chiral structure; when the laser beam is directed at this part (Trap 3), the structure rotates around the x -axis (Figure 1(a)). Thus, the microrobot only rotates when the third laser beam is activated. The optical handles are ellipsoidal to minimize drag during the robot’s translation, and the front handle has a tip to be used later for drilling purposes. It should be noted that Trap 3 is off-axis compared to Trap 1 and Trap 2 and does not point to the center of the robot axis but is offset by about $1.2 \mu\text{m}$.

The optomechanical behaviour of this design was studied by finite element methods using COMSOL Multiphysics software (for more details, see Methods section). A linearly-polarized Gaussian beam with wavelength 1070 nm propagating in the z -direction was directed to the chiral part. Electromagnetic Maxwell stress tensor (MST) was calculated for the helix with different angles of rotation from 0 to 120 degrees around the x -axis as its shape exhibits rotational symmetry of order 3 as depicted in Figure 1 (b). Then, MST was implemented in the structural mechanics module to calculate the generated optical force and torque on the microrobot (see Methods Section). Our calculations assume that the two traps on the optical handle generate a stable stiffness and prevent any motion except the rotation along the x -axis. The electric field distribution shows breaking the axial parity as it interacts with the chiral geometry leading to an unsymmetric stress distribution within the structure. Consequently, a torque is generated, initiating rotational motion in the same direction of the helix chirality. As shown in Figure 1b, the generated torque is always positive and the robot should not exhibit any reverse rotations. The torque varies according to the angle; this can be attributed to the contribution of the scattering field for different positions. When a part of the helix is in direct contact with the focal point the laser power is the highest and hence the optical force and torque are maximal. Finally, for clarity, we depict the norm of the MST on the surface of the helix for different position angles of the structure in Figure 1(c) and in the xz -plane.

3 Experimental Demonstration

The microrobots were fabricated by three-dimensional direct laser writing based on the two-photon absorption lithography technique which is a high-resolution 3D printing process that utilizes a femtosecond laser to induce polymerization at the focal point within a photosensitive resin (see Methods section). This technique relies on the simultaneous absorption of two photons, which provides the energy necessary to initiate polymerization only at the precise focal spot. As a result, this technique enables the creation of intricate microstructures with sub-micrometer resolution. By scanning the laser focal point in three dimensions, complex 3D micro- and nano-structures can be constructed layer by layer, making it an ideal method for fabricating sophisticated microrobots. Therefore, we were able to fabricate the designed microrobots with high resolution (see Figure 2). The printing was done layer-by-layer along the optobot’s longest axis; and a thin pillar with 660 nm diameter is printed under the helix to connect the optobots to the substrate. Therefore, all the robots were supposed to be standing vertically over the pillar connected to the substrates. The SEM images demonstrate different robots with side view angle of 45° to show the robots standing on the substrates, and a zoomed picture to show the whole body clearly including its different components: the helix that was printed with high resolution and without any adhesion between its parts, the pillar and the optical handles where the front one has a thin indentation to help in drilling later; this part was also printed with high resolution; although its diameter is around 200 nm. We also depict the top view of a standing robot that only shows the head and part of the helix, and a top view of another robot with its pillar detached from the substrate.

The Optobot was actuated by three laser beams (same beam but switching the trapping position); two for trapping the optical handles, and the third one for rotating the chiral helix. The process begins with activating the first two traps to hold the micro-robot and control its position; then, the third trap is activated to start the rotation. This led to the rotation of the microrobot around its longer axis in the out-of-plane direction with an angular frequency of about 0.15 Hz (Figure 3, video S1). The rotation can

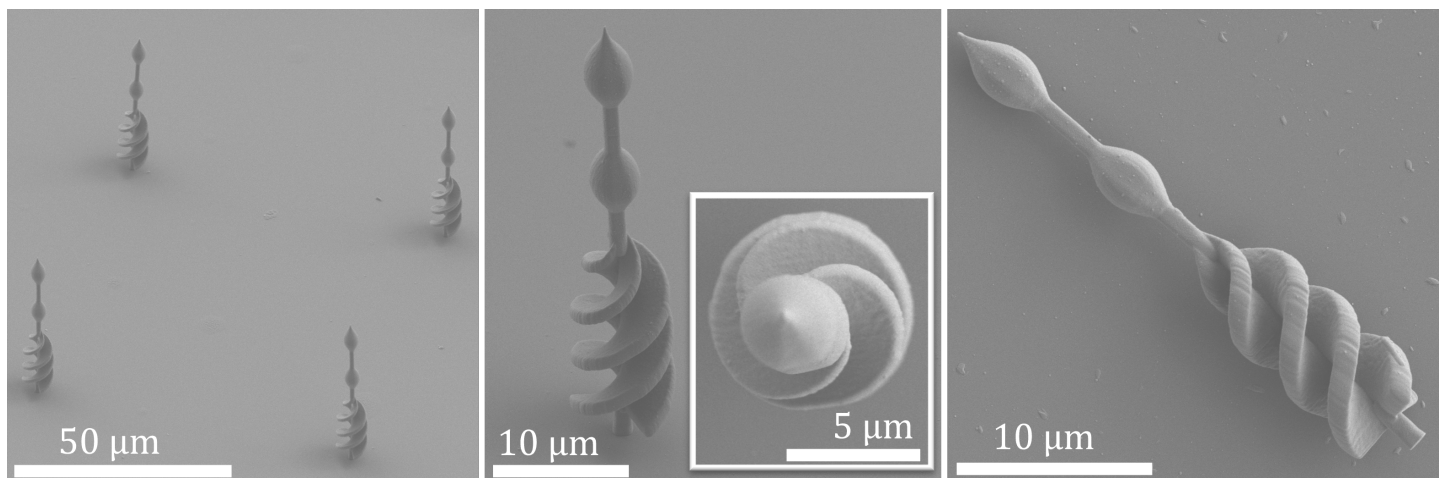


Figure 2: SEM images of the optical drill fabricated using two-photon lithography printing technique. The robots were printed to be standing vertically over the pillar connected to the substrates. We show an array of robots standing perpendicularly to the substrate, a top and tilted view with an angle of 45° of a standing robot. In addition to a top-view of a robot detached from the substrate to show clearly the printing of the different components of the Optobot; the helix, optical handles, and the indentation at the front optical handle to do the drilling.

be turned on and off according to the activation or deactivation of the third trap (video S2). Moreover, the rotation can be maintained while the microrobot is fixed or moving (video S3). The ability to control the microrobot with different options and capabilities is highly advantageous for various applications. The precise manipulation of the microrobot's rotation and movement allows for an efficient and targeted drilling process. By selectively activating and deactivating the laser traps, it is possible to tune the microrobot's actions to meet specific requirements. This level of control enhances the versatility of the microrobot, making it suitable for complex tasks in microfabrication and minimally invasive medical procedures. The capability to maintain rotation while the microrobot is either fixed or in motion adds an extra dimension of functionality, ensuring consistent performance in dynamic environments. This controlled and adaptable system paves the way for advanced operations where precision and flexibility are required, leading to more efficient and effective outcomes in microscale drilling and beyond.

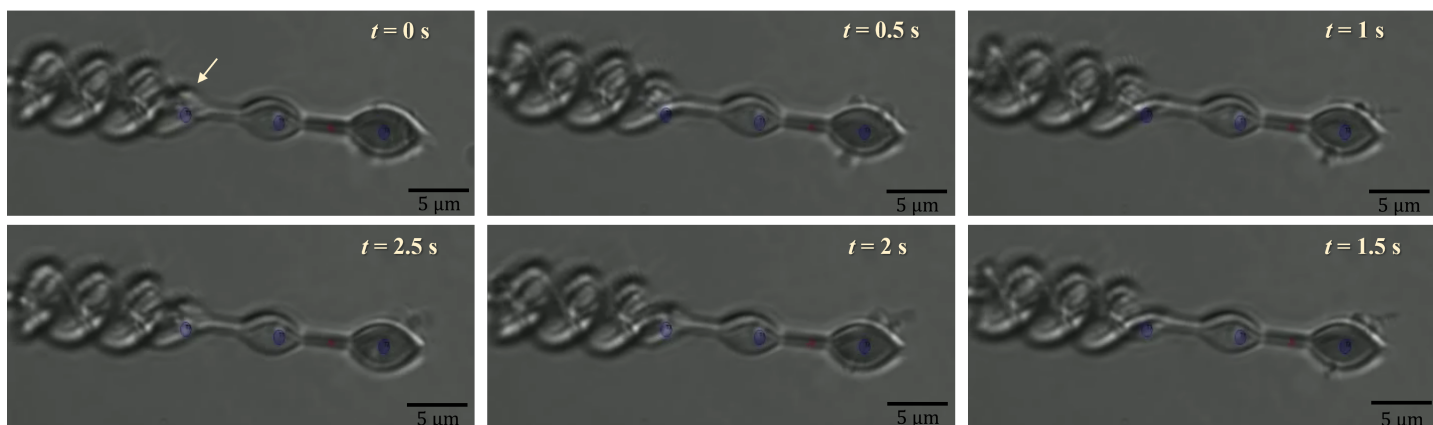


Figure 3: Optical images of the Optical Drill during one third of the rotational cycle. Snapshots are taken from a video (see Supplemental files) for different times during the rotation of the optobot when the third trap is focused on the chiral part while the two other traps are used for keeping the robot in place. To track the rotation, the first turn of the helix (indicated by an arrow in the first picture) was followed. The, robot gets a similar configuration after 2.5 s; which indicates a third of a rotational cycle due to the C3 symmetry of the robot.

4 Conclusion

In this paper, we have utilized a chiral broken axial parity to achieve continuous rotation of an optobot upon optical illumination. Specifically, we accomplished repetitive rotation by employing three focal regions on the optobot: two traps to stabilize its position and one focal point on the chiral part to induce rotation. The fabricated structure, designed using the finite element method, demonstrated highly satisfactory performance during optical testing, closely matching our theoretical predictions.

Methods Section

Fabrication

The microrobots were fabricated by a commercial 3D printer (Photonic Professional GT+, Nanoscribe GmbH) utilizing the two photon lithography technique. The photoresin chosen for the fabrication was the commercial IP-L 780 negative resist (Nanoscribe GmbH) that can be used to print in oil immersion configuration over borosilicate D263 substrates with a thickness of $170\mu\text{m} \pm 10\mu\text{m}$; which could be used later for the optical tweezer system. Moreover, IP-L 780 provides high resolution where the smallest feature that can be printed using it is 200nm. The slicing and hatching distances were both equal to $0.1\mu\text{m}$. A drop of the resist was deposited on the substrate and photopolymerized with a femtosecond laser operating at $\lambda = 780\text{nm}$ and a 63X objective in oil immersion configuration. A laser power of 50 percent and a galvanometric scan speed of $4000\mu\text{m/s}$ were used for the whole fabrication process. The robots were printed vertically to decrease the adhesion to the substrate, and a small pillar was printed at the bottom side of the helix to connect the robot to the substrate. After printing, the sample was developed for 12 minutes in a propylene glycol methyl ether acetate (PGMEA) solution in order to remove all the unexposed photoresist. The sample was further rinsed two times for 3 minutes in isopropyl alcohol (IPA) to clear the developer. In order to dry these 3D delicate microrobots efficiently, critical point drying was used (Autosamdri 931, Tousimis).

SEM Imaging

The fabricated structures were examined with an ApreoS ThermoFisher SEM in Optiplan mode. To achieve high-quality imaging, the surface was pre-coated with a thin layer of chromium using a Leica ACE600 sputter coater, achieving a chromium thickness of less than 5 nm. The imaging voltage was maintained below 10 kV to prevent damage to the structures. The images are done on theoretically identical structures used for the optical experiments; however, they are not the same. We cannot use the structures with metal on them for the experiment.

Finite Element Method

We employed the finite elements software COMSOL Multiphysics, to explore the intricate interactions between a Gaussian beam and optobots. Our primary objective was to determine the resultant forces and displacements experienced by the optobots when subjected to this beam. First, we meticulously computed all components of the Maxwell stress tensor (MST).

MST is a fundamental concept in electromagnetism that describes the flow of electromagnetic momentum through space. It encapsulates the effects of electric and magnetic fields on the mechanical stress within a medium. The tensor is particularly useful in calculating the force and torque on objects due to electromagnetic fields.

MST, denoted as \mathbf{T} , is a second-rank tensor given by:

$$T_{ij} = \epsilon_0 \left(E_i E_j - \frac{1}{2} \delta_{ij} E^2 \right) + \frac{1}{\mu_0} \left(B_i B_j - \frac{1}{2} \delta_{ij} B^2 \right) \quad (1)$$

where ϵ_0 is the permittivity of free space, μ_0 is the permeability of free space, E_i and E_j are the components of the electric field vector \mathbf{E} , B_i and B_j are the components of the magnetic field vector \mathbf{B} , and δ_{ij} is the Kronecker delta, which is 1 if $i = j$ and 0 otherwise.

MST allows us to compute the electromagnetic force \mathbf{F} on a particle by integrating the tensor over the surface \mathbf{S} , and accordingly the torque, $\boldsymbol{\tau}$, can be calculated.

$$\begin{aligned}\mathbf{F} &= \oint_S \mathbf{T} \cdot d\mathbf{S} \\ \boldsymbol{\tau} &= \mathbf{r} \times \mathbf{F}\end{aligned}\quad (2)$$

where $d\mathbf{S}$ is the differential area vector on the surface. The divergence of the MST also relates to the force density in a region, providing a comprehensive framework for understanding the interaction between electromagnetic fields and mechanical forces.

Following this, we leveraged the structural mechanics module within COMSOL to determine the displacement of the chiral component of the Optobot. For this analysis, we assumed that the two other traps (trap 1 and trap 2) in the setup constrain the Optobot, allowing it to rotate around the x -axis. This assumption simplifies the model and focuses on the rotational dynamics of the chiral part, which is crucial for understanding its behavior under the influence of the Gaussian beam. The normalized torque was calculated as a ratio of the maximum achievable optical torque (τ_{\max}) [34, 31] calculated according to equation 3.

$$\tau_{\max} = P \cdot n_m \cdot r / c \quad (3)$$

Where P is the laser power, n_m is the refractive index of the medium around the optobot which is water of $n_m = 1.33$, r is the radius of the part of the helix interacting with the laser beam, and c is the light velocity.

Optical Testing

The optical tweezer platform integrates an optical setup, a moving stage, and a controller device. The optical setup, built around a custom inverted microscope with an oil immersion objective (Olympus UPlanFLN 40X, NA 1.3), uses a near-infrared laser source (1070nm). Visual feedback is provided by LED illumination reflected in a high-speed CMOS camera (Basler, 659×494 px). The system employs two actuation methods: a 3D nano-stage (PI P-562.3CD) on a 2D micro-stage (PI M-126.CGX) for large workspace and fine control, and high-speed laser deflection via a galvanometer (GVS002, Thorlabs) and a deformable mirror (PTT111 DM, Iris AO) for dynamic time-sharing multi-trap positioning. This setup allows for precise sample manipulation using the controller device while keeping trapped objects stationary, combining passive and active actuation for improved control [18].

For the separation of the microrobots from the substrate, an experimental setup is centered around a commercial microscope (OPTIKA). It includes a three-axis micromanipulator system (MP-285, Sutter Instrument). A micro-pipette (Borosilicate glass capillary, B150-110-10) was adjusted using a micropipette puller (Sutter instruments, Model P-1000 Flaming Brown Micropipette Puller) to get a tip of diameter around $2\mu\text{m}$; then it was attached to the micromanipulator system which was used to precisely control the micro-pipette movement and observe its movement under the microscope to push the microrobots one by one and separate them from the substrate to be freely swimming in water with 5% tween20 to avoid adhesion of the robots to each other, or re-adhesion to the substrate (video S4).

Supporting Information

Supporting Information is available from the Wiley Online Library or the authors.

Acknowledgements

The authors acknowledge the support ANR OPTOBOTS project (ANR-21-CE33-0003), M.K. and B.L. thank the ANR PNanoBot (ANR-21-CE33-0015). The work was supported by the French RENATECH network and its FEMTO-ST technological facility MIMENTO.

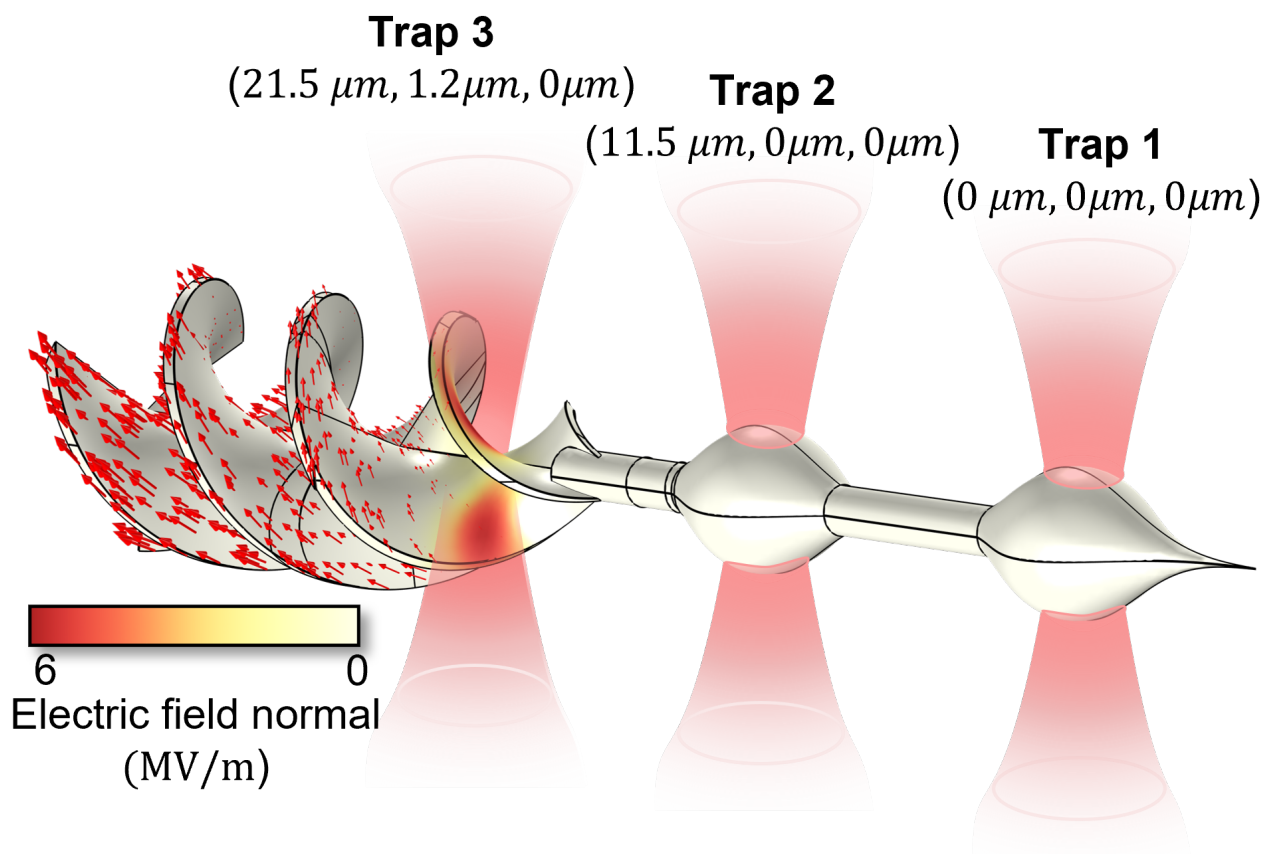
This work has been achieved in the frame of the EIPHI graduate school (contract "ANR-17-EURE-0002")

References

- [1] J. D. Jackson, *Electrodynamics, Classical*, John Wiley & Sons, Ltd, ISBN 9783527600434, **2003**.
- [2] D. Arslan, A. Rahimzadegan, S. Fasold, M. Falkner, W. Zhou, M. Kroychuk, C. Rockstuhl, T. Pertsch, I. Staude, *Advanced Materials* **2022**, *34*, 5 2105868.
- [3] R. Alaei, M. Kadic, C. Rockstuhl, A. Passian, *Applied Physics Letters* **2016**, *109*, 14.
- [4] R. Alaei, J. Christensen, M. Kadic, *Physical Review Applied* **2018**, *9*, 1 014007.
- [5] A. Ashkin, *Phys. Rev. Lett.* **1970**, *24* 156.
- [6] A. Ashkin, *Phys. Rev. Lett.* **1970**, *25* 1321.
- [7] A. Ashkin, J. M. Dziedzic, J. E. Bjorkholm, S. Chu, *Optics Letters* **1986**, *11*, 5 288.
- [8] R. C. Sullivan, H. Boyer-Chelmo, K. Gorkowski, H. Beydoun, *Accounts of Chemical Research* **2020**, *53*, 11 2498.
- [9] Y. Shen, D. A. Weitz, N. R. Forde, M. Shayegan, *Soft Matter* **2022**, *18* 5359.
- [10] Zaltron, Annamaria, Merano, Michele, Mistura, Giampaolo, Sada, Cinzia, Seno, Flavio, *Eur. Phys. J. Plus* **2020**, *135*, 11 896.
- [11] O. M. Maragò, P. H. Jones, P. G. Gucciardi, G. Volpe, A. C. Ferrari, *Nature nanotechnology* **2013**, *8*, 11 807—819.
- [12] J. Melzer, E. McLeod, *Microsystems and Nanoengineering* **2021**, *7*, 1.
- [13] E. Mcleod, C. B. Arnold, *Optics Express* **2009**, *17* 5 3640.
- [14] E. Mcleod, C. B. Arnold, *Nature nanotechnology* **2008**, *3* 7 413.
- [15] A. Kaufman, K.-K. Ni, *Nature Physics* **2021**.
- [16] Y. Zhang, C. Min, X. Dou, X. Wang, H. P. Urbach, M. G. Somekh, X. Yuan, *Light, Science & applications* **2021**, *10*, 1 59.
- [17] J. Gieseler, J. Millen, *Entropy* **2018**, *20*, 5 326.
- [18] E. Gerena, F. Legendre, A. Molawade, Y. Vitry, S. Régnier, S. Haliyo, *Micromachines* **2019**, *10*, 10.
- [19] D. Zhang, A. Barbot, B. Lo, G.-Z. Yang, *Advanced Optical Materials* **2020**, *8*, 21 2000543.
- [20] A. Ashkin, K. Schütze, J. Dziedzic, U. Euteneuer, M. Schliwa, *Nature* **1990**, *348*, 6299 346—348.
- [21] K. I. Schimert, W. Cheng, *Proceedings of SPIE—the International Society for Optical Engineering* **2018**, *10723* 107233B.
- [22] Z. Zhang, T. E. P. Kimkes, M. Heinemann, *Scientific Reports* **2019**, *9*, 1 19086.
- [23] T. Hayakawa, S. Fukada, F. Arai, *IEEE Transactions on Robotics* **2014**, *30* 59.
- [24] S. Hu, R. Hu, X. Dong, T. Wei, S. Chen, D. Sun, *Opt. Express* **2019**, *27*, 12 16475.
- [25] P.-K. Andrew, A. Raudsepp, D. Fan, U. Staufer, M. A. K. Williams, E. Avci, *Opt. Express* **2021**, *29*, 16 25836.
- [26] E. Gerena, S. Régnier, S. Haliyo, *IEEE Robotics and Automation Letters* **2019**, *4*, 2 647.
- [27] E. Avci, M. Grammatikopoulou, G.-Z. Yang, *Advanced Optical Materials* **2017**, *5*, 19 1700031.

- [28] T. Asavei, T. Nieminen, V. Loke, A. Stilgoe, R. Bowman, D. Preece, M. Padgett, N. Heckenberg, H. Rubinsztein-Dunlop, *New Journal of Physics* **2013**, *15* 063016.
- [29] D. J. Collins, F. S. Ligler, *Lab on a Chip* **2017**, *17* 591.
- [30] A. Rahimzadegan, M. Fruhnert, R. Alaei, I. Fernandez-Corbaton, C. Rockstuhl, *Phys. Rev. B* **2016**, *94* 125123.
- [31] S. Bianchi, G. Vizsnyiczai, S. Ferretti, C. Maggi, R. Leonardo, *Nature Communications* **2018**, *9*.
- [32] L. Anderson, S. Kirchner, D. Schamel, P. Fischer, T. Lohmüller, J. Feldmann, In *2014 Conference on Lasers and Electro-Optics (CLEO) - Laser Science to Photonic Applications*. **2014** 1–2.
- [33] P. Galajda, P. Ormos, *Applied Physics Letters* **2002**, *80*, 24 4653.
- [34] A. Rahimzadegan, R. Alaei, I. Fernandez-Corbaton, C. Rockstuhl, *Phys. Rev. B* **2017**, *95* 035106.

Table of Contents



Principle of an optical drill controlled via three optical traps.